10

Iris Pattern Classification Combining Orientation Recognition

Hironobu Takano and Kiyomi Nakamura
Toyama Prefectural University
Japan

1. Introduction

The importance of personal authentication is gradually increasing with the development of the information society. Biometrics identification technology plays an important role in cyberspace. Unlike other biometrics such as the face or fingerprints, iris recognition has high reliability for personal identification. Iris recognition methods are classified into four categories: the phase-based method (Daugman, 1993), the zero-crossing representation-based method (Boles and Boashash, 1998; Sanchez-Avila and Sanchez-Reillo, 2005), the texture-based method (Wildes, 1997; Ma et al., 2003), and local intensity variation (Ma et al., 2004, a;b). Using the internal CASIA dataset (CBSR, 2005), Ma et al. evaluates the proposed algorithm by comparing the performance of other iris recognition methods proposed by Daugman, Wildes, and Boles and Boashash (Ma et al., 2004, b). The experimental results show the equal error rates (EER) of respective algorithms (Ma, Daugman, Wildes, and Boles) are 0.07%, 0.08%, 1.76%, and 8.13%, respectively. In other studies, the Daugman's method which is a representative algorithm of iris recognition is also evaluated using the subset of internal CASIA dataset (Sun et al., 2006) and the CASIA iris image 1.0 database (Wang et al., 2007), which is available from the CASIA web site. The EERs of Daugman's method reported in Sun et al. and Wang et al. are 0.70% and 0.67%, respectively. These analysis indicate the high accuracy of recognition performance although the EERs of Daugman's method described in these papers are not the same because the iris segmentation method including eyelid and eyelash detection would not be exactly the same.

Iris recognition technology are applied in various fields. Especially, the iris recognition algorithm embedded on a mobile phone requires robustness to rotation changes because capturing the iris pattern by a hand using a camera built in the mobile phone causes the rotation changes. However, the iris recognition methods described above are generally fragile in rotation variation.

We previously proposed a rotation spreading neural network (R-SAN net) that focused on spatial recognition/memory systems (parietal cortex(PG)) in the brain and recognized an object's orientation and shape (Nakamura et al., 1998; Yoshikawa and Nakamura, 2000). The R-SAN net can simultaneously recognize the orientation of the object irrespective of its shape, and the shape irrespective of its orientation. The characteristics of the R-SAN net are to use a two-dimensional input pattern in a polar coordinate system converted from the Cartesian coordinate system. The R-SAN net is suitable for the shape and orientation recognition of concentric circular patterns. The orientation recognition performance of R-SAN net allows the

accurate compensation of the orientation variation. In addition, the R-SAN net has the unique characteristics of orientation recognition. The recognized orientation for unlearned irises was heavily dispersed from the orientation of input iris although the orientation for learned irises was concentrated around input orientation. By combining the orientation recognition characteristics, a novel iris recognition method was developed.
On the other hand, despite the high recognition accuracy, the iris authentication system is vulnerable to deception by fake irises (Matsumoto et al., 2004). Thus, the iris recognition system requires liveness detection for discriminating between live and fake irises. For discriminating between live and fake irises, many liveness detection methods have been proposed earlier, for example, the eye gaze detection method, pupillary reflex method, etc. (Tachibana, 2006; Tsukahara, 2006; Oda, 2000; Kobayashi et al., 2005). The eye gaze detection method constrains the user to move their eyes along with the movement of a marker displayed on a screen. In the liveness detection method using corneal reflection of near-infrared light, an imposter can imitate an iris by painting an artificial corneal reflection image on the iris image. The pupillary reflex method uses the variations in the pupil size with time as a result of flashlight illumination. However, in these methods, biometric data for the identification of an individual and liveness data for classifying live and fake irises are obtained by measuring different physical features. To increase the reliability of liveness detection, we developed a novel liveness detection method using the brightness variation of the iris pattern based on pupillary reflex (Kanematsu et al., 2007).
In this chapter, we introduce the recognition method using the characteristics of orientation recognition for decreasing false acceptance. We also show a novel liveness detection for discriminating the live and fake irises. Section 2 describes the structure of the rotation spreading neural network (R-SAN net). The outline of the real-time iris recognition system using R-SAN net is shown in Section 3. Recognition performance of the iris pattern and orientation are evaluated in Section 4. Section 5 details the iris recognition method which introduces the unlearned iris rejection with the orientation recognition characteristics. The liveness detection method is described in Section 6. Section 7 concludes this chapter.

2. Rotation spreading neural network

2.1 Structure of the R-SAN net

The structure of the R-SAN net is shown in Fig.1. The R-SAN net consists of orientation and shape recognition systems. In the operation of this net, the input pattern (300×300 pixels) is converted to a transformed pattern on the polar coordinates. This transformed pattern is input into the spreading layer, and the spread pattern $\boldsymbol{V}$ is obtained.
In learning, the spread pattern $\boldsymbol{V}_{\mathrm{L}}^{(P)}$ is obtained by using the *P-th* learning input pattern in the spreading layers. The orientation memory matrix $\boldsymbol{\mathcal{M}}_{\mathrm{O}}$ is obtained by associating $\boldsymbol{V}_{\mathrm{L}}^{(P)}$ with the desired outputs of orientation recognition neurons $\boldsymbol{TO}^{(P)}$. The $\boldsymbol{\mathcal{M}}_{\mathrm{O}}$ and $\boldsymbol{V}_{\mathrm{L}}^{(P)}$ are stored in the iris recognition system. In recognition, the output of orientation recognition neurons $\boldsymbol{YO}$ is obtained by multiplying the spread pattern $\boldsymbol{V}_{\mathrm{R}}^{(P)}$ by orientation memory matrix $\boldsymbol{\mathcal{M}}_{\mathrm{O}}$. The orientation is recognized from the output of orientation recognition neurons using the population vector method (Georgopoulus et al., 1982). The shape (iris pattern) is discriminated with the Euclidean distance between the spread patterns obtained in learning and recognition processes.

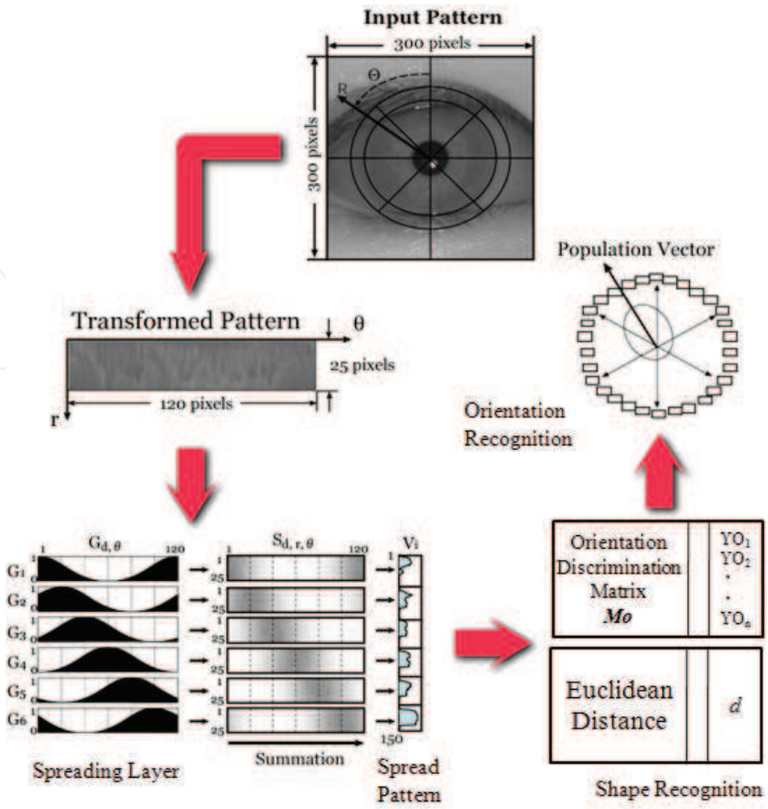

Fig. 1. Structure of the R-SAN net.

2.2 Generation of a transformed image

The original image for learning and recognition is a gray scale image of 300×300 pixels. The transformed image is made by sampling the original image on the polar coordinates (r, θ) at every 3 degrees in θ and at equal intervals of 25 pixels in radius r excluding the pupil area. In order to get an accurate value of the transformed $T_{r,\theta}$, the small sampling region is further divided into 3×3 points and the pixel value of each point is summed. This transformed image is generated by Eq.(1), where $I_{x,y}$ is the pixel value of the original image at (x, y) on the Cartesian coordinates, and $T_{r,\theta}$ is the pixel value of the transformed image at (r, θ) on the polar coordinates. Example of the original and transformed images is shown in Fig.2 (a) and (b).

$$T_{r,\theta} = \sum_{i=1}^{3} \sum_{j=1}^{3} I_{x,y} \tag{1}$$

$$(x = R\cos\Theta, \;\; y = R\sin\Theta)$$

$$\left(R = (r-1) + \frac{i}{3}, \;\; \Theta = \left\{(\theta - 1) + \frac{j}{3}\right\} \times 3\right)$$

2.3 Spreading layers

The structure of the spreading layers is shown in Fig.3. As shown in Eq.(4), the spread image $S_{d,r,\theta}$ corresponding to the respective spreading weight is obtained by multiplication of the

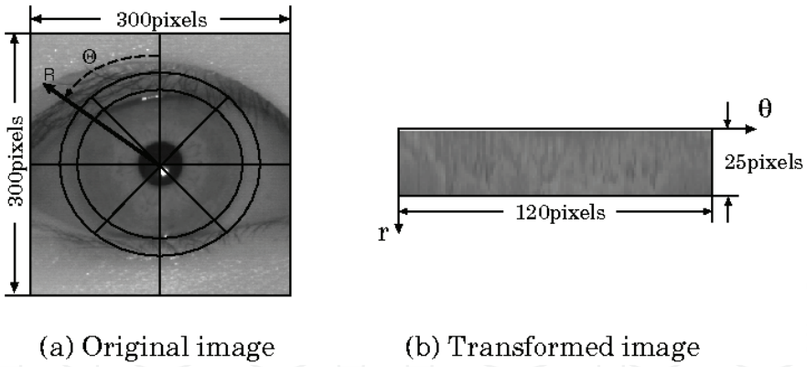

Fig. 2. Example of original and transformed images.

transformed image $T_{r,\theta}$ with the spreading weight $G_{d,\theta}$, which is the periodic Gaussian curve function predetermined at equal intervals in the θ direction (Eqs.(2) and (3)). The spread image is summed in the θ direction and combined to produce the spread pattern vector $\boldsymbol{V}^*$ (Eqs.(5) and (6)).

$$F_S(x) = \exp\left\{-\beta(x-120n)^2\right\} \tag{2}$$
$$(-60+120n < x \leq 60+120n, n = 0, \pm 1, \ldots)$$
$$G_{d,\theta} = F_S\left\{20(d-1)-(\theta-1)\right\} \tag{3}$$
$$(d = 1, 2, \cdots, 6\ ,\ \theta = 1, 2, \cdots, 120)$$
$$S_{d,r,\theta} = T_{r,\theta} \times G_{d,\theta} \tag{4}$$
$$(r = 1, 2, \cdots, 25)$$
$$V_i^* = \sum_{\theta=1}^{120} S_{d,r,\theta} \qquad (i = 25(d-1)+r) \tag{5}$$
$$\boldsymbol{V}^* = [V_1^*, \cdots, V_{150}^*]^T \tag{6}$$

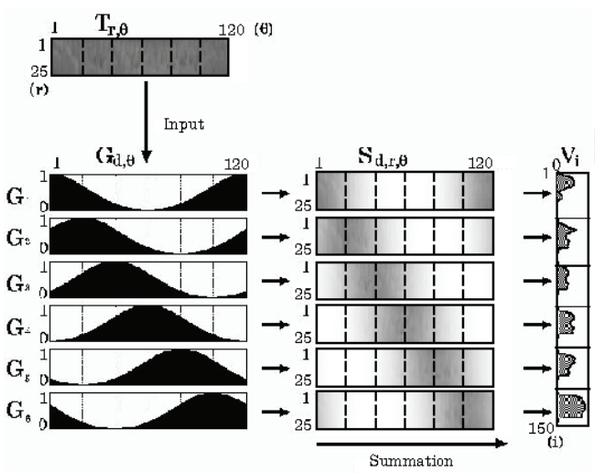

Fig. 3. Structure of the spreading layers.

To remove the bias of V^* which degrades the recognition performance, the normalized spread pattern vector V is obtained by Eqs.(7) and (8). As a feature vector of the iris pattern, the normalized spread pattern V is used for both learning and recognition.

$$||V^*|| = \sqrt{\sum_{i=1}^{150} V_i^{*2}} \tag{7}$$

$$V = \frac{V^*}{||V^*||} \tag{8}$$

2.4 Teaching signal

The teaching signal for orientation recognition is shown in Fig.4. Orientation recognition neurons YO_i $(i = 1, 2, \cdots, 30)$ are arranged at equal intervals of orientation. There are six learning signals $\boldsymbol{KO}^{(d)}$ corresponding to the six orientations d to be memorized. The desired outputs of the orientation recognition neurons are broadly tuned to the orientation of an iris pattern and adjusted to the function in Eq.(9). The desired outputs of orientation recognition neurons $\boldsymbol{TO}^{(P)}$ in Eq.(11) are fitted to $\boldsymbol{KO}^{(d)}$ which is the Gaussian curve function defined by Eqs.(9) and (10). Here, P is the learning pattern number and d is learning orientations $(O1 \sim O6)$. α is the learning coefficient that defines the tuning width of the teaching signal of orientation recognition neurons. The learning coefficient, α, is determined so that an orientation recognition neuron corresponding to the learning orientation outputs a peak value 1.0, and the orientation recognition neurons corresponding to the nearest neighbor learning directions output 0.5. The orientation $(O1 \sim O6)$ of iris images rotated every 60 degrees are learned.

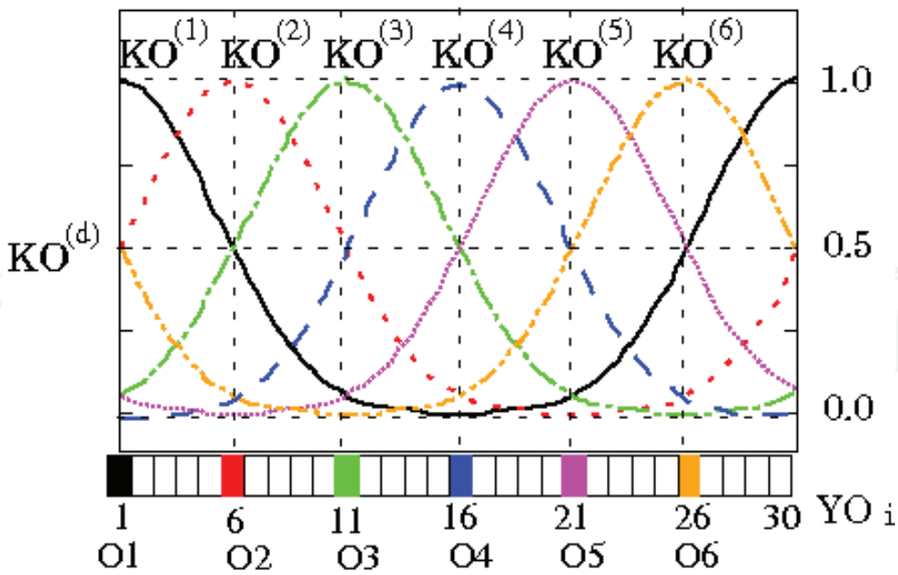

Fig. 4. Teaching signal for orientation recognition.

$$F_O(x) = \exp\left\{-\alpha(x-30n)^2\right\} \tag{9}$$

$$(-15+30n < x \leq 15+30n, n = 0, \pm 1, \ldots)$$

$$YO_i^{(P)} = KO_i^{(d)} = F_O\left\{5(d-1)-(i-1)\right\} \tag{10}$$

$$(d = 1, 2, \cdots, 6\ ,\ i = 1, 2, \cdots, 30)$$

$$\boldsymbol{TO}^{(P)} = \boldsymbol{KO}^{(d)} = [KO_1^{(d)}, KO_2^{(d)}, \cdots, KO_{30}^{(d)}]^T \tag{11}$$

2.5 Population vector method

The orientation of the iris pattern is indicated by the angle of a population vector ϕ. The ϕ is defined as an ensemble of vectors of the orientation recognition neurons $\boldsymbol{YO} = [YO_1, \cdots, YO_{30}]^T$ where each vector points to the neuron's optimally tuned orientation and has a length in proportion to the neuron's output (Georgopoulus et al., 1982). The arrangement of orientation neurons and the orientation population vector are shown in Fig.5. This assumes that the neurons in the parietal cortex recognize the axis orientation of an object by population coding, as seen in neurophysiological studies. Each orientation recognition neuron YO_i has a respective representative orientation ψ_i that characterizes the best orientation for the optimal response in Eq.(12). The population vector orientation ϕ is calculated by the vectorial summation of 30 orientation neurons $(YO_1, \cdots, YO_{30})$ by Eqs.(13) and (14).

$$\psi_i = \frac{2\pi}{30} \times (i-1) \quad [\text{rad}] \tag{12}$$

$$(i = 1, 2, \cdots, 30)$$

$$\begin{aligned} x &= \sum_{i=1}^{30} YO_i \cos\psi_i \\ y &= \sum_{i=1}^{30} YO_i \sin\psi_i \end{aligned} \tag{13}$$

$$\phi = \tan^{-1}\left(\frac{y}{x}\right) \tag{14}$$

2.6 Learning process

The R-SAN net uses generalized inverse learning for orientation recognition (Amari, 1978). The spread pattern $\boldsymbol{V}_{\mathrm{L}}^{(P)}$ is obtained from the *P-th* learning input pattern in the spreading layers. The orientation memory matrix $\boldsymbol{\mathcal{M}}_{\mathrm{O}}$ is obtained by associating $\boldsymbol{V}_{\mathrm{L}}^{(P)}$ with the desired outputs of orientation recognition neurons $\boldsymbol{TO}^{(P)}$ by Eq.(17). The number of learning patterns is given by multiplying the number of learning irises by the number of learning orientations for each iris. For example, when the number of learning irises is 10 and the number of learning orientations is 6, it is 10 (irises) $\times$ 6 (orientations) = 60 (patterns). For iris pattern learning, the

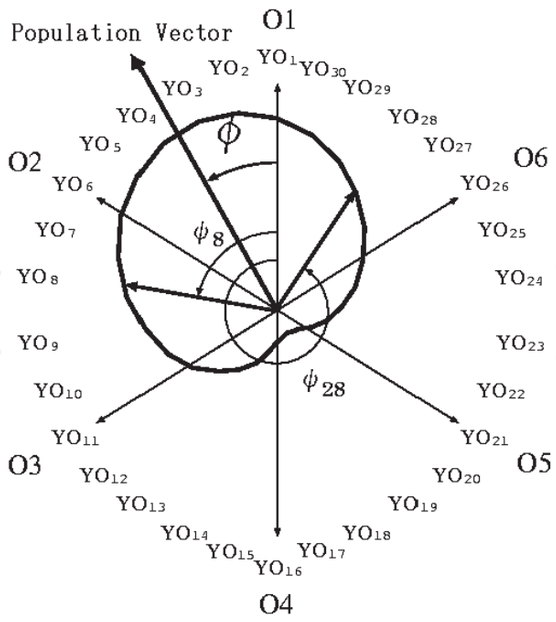

Fig. 5. Arrangement of orientation recognition neurons in population vector method.

spread patterns $\boldsymbol{V}_{\mathrm{L}}^{(P)}$ for the respective irises are registered in the iris recognition system.

$$\boldsymbol{\mathcal{X}} = [\boldsymbol{V}_{\mathrm{L}}^{(1)}, \boldsymbol{V}_{\mathrm{L}}^{(2)}, \cdots, \boldsymbol{V}_{\mathrm{L}}^{(60)}] \tag{15}$$

$$\boldsymbol{\mathcal{X}}^{\dagger} = (\boldsymbol{\mathcal{X}}^{T}\boldsymbol{\mathcal{X}})^{-1}\boldsymbol{\mathcal{X}}^{T} \tag{16}$$

$$\boldsymbol{\mathcal{M}}_{\mathrm{O}} = \boldsymbol{\mathcal{TO}}\boldsymbol{\mathcal{X}}^{\dagger} \tag{17}$$

$$\boldsymbol{\mathcal{TO}} = [\boldsymbol{TO}^{(1)}, \boldsymbol{TO}^{(2)}, \cdots, \boldsymbol{TO}^{(60)}]$$

2.7 Recognition process

In recognition, the spread iris pattern $\boldsymbol{V}_{\mathrm{R}}$ used in recognition is generated from an input iris image. For orientation recognition, the output of orientation recognition neurons $\boldsymbol{YO} = [YO_1, \cdots, YO_{30}]^T$ is obtained by multiplying the spread pattern $\boldsymbol{V}_{\mathrm{R}}$ by orientation memory matrix $\boldsymbol{\mathcal{M}}_{\mathrm{O}}$ in Eq.(18). The orientation of the input iris pattern is recognized from the output of orientation recognition neurons using the population vector method. This method provides the orientation of the iris pattern by synthesizing the continuous spectra of the outputs of the orientation recognition neurons.

$$\boldsymbol{YO} = \boldsymbol{\mathcal{M}}_{\mathrm{O}}\boldsymbol{V}_{\mathrm{R}} \tag{18}$$

The shape (iris pattern) is discriminated with the Euclidean distance between the spread patterns obtained in learning and recognition processes. The value of Euclidean distance d in Eq.(19) has the range of $0 \leq d \leq 2$, because the norm of spread pattern $||\boldsymbol{V}||$ are normalized as "1". In Eq.(19), $\boldsymbol{V}_{\mathrm{L}}$ and $\boldsymbol{V}_{\mathrm{R}}$ correspond to the normalized spread pattern of 0° during learning and during recognition, respectively. When it has the Euclidean value of "0", resemblance is the highest.

$$d = ||\boldsymbol{V}_{\mathrm{L}} - \boldsymbol{V}_{\mathrm{R}}|| \tag{19}$$

3. Real-time iris recognition system

3.1 System configuration

The configuration of the real-time iris recognition system is shown in Fig.6. The system consists of a near-infrared CCD camera, PC, near-infrared lighting, and flash-light generation equipment. The PC has an image input board to acquire the iris images and DLL (Dynamic Link Library) software for processing iris images. The flash-light generation equipment emits a flash using an external trigger signal synchronized with the arbitrary input image frame. The near-infrared lighting provides clear iris images for the CCD camera. A fixed-size pupil image can be obtained by utilizing the pupillary reflex caused by illuminating the same eye. The pupillary reflex is also used for liveness detection. The input iris images captured by the CCD camera are gray-scaled images of 640 $\times$ 480 pixels every 1/30 sec.

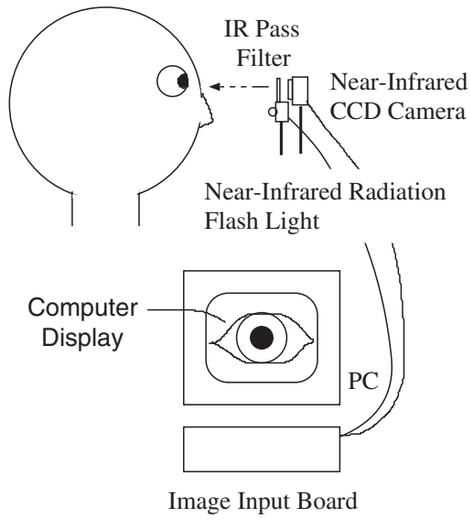

Fig. 6. Configuration of iris recognition system.

3.2 Outline of the iris recognition system

The flowchart of the iris recognition system is shown in Fig.7. First, the template matching method with a partial eye template detects the pupil position from the eye image continuously taken by the near-infrared CCD camera (Miyazaki et al., 2007). After detection of the pupil location, variations of pupil size (diameter) due to pupillary reflex are measured by calculating the average distance between the center of pupil compensated by the labeling and least squared fitting method and pixels on the circumference. The iris size (diameter) is measured by edge detection using the Prewitt filter. Although the measurement sizes of the iris and pupil in the image change with the magnification of a lens and the distance between the camera and eye, the iris and pupil sizes (diameter) can be accurately measured using the characteristics of the fixed (almost equal) iris size without individual differences. The variation of pupil size (diameter) during pupillary reflex induced by using a weak LED-flashlight is shown in Fig.8. When the pupil diameter normalized by the measured iris diameter is between 2.9 mm and 3 mm as shown in Fig.8, the eye image is taken as a standard image of the iris and pupil. A 300 $\times$ 300 pixel image including the iris pattern is extracted from this eye image, which is zoomed using the linear interpolation. Thus, the pupil size

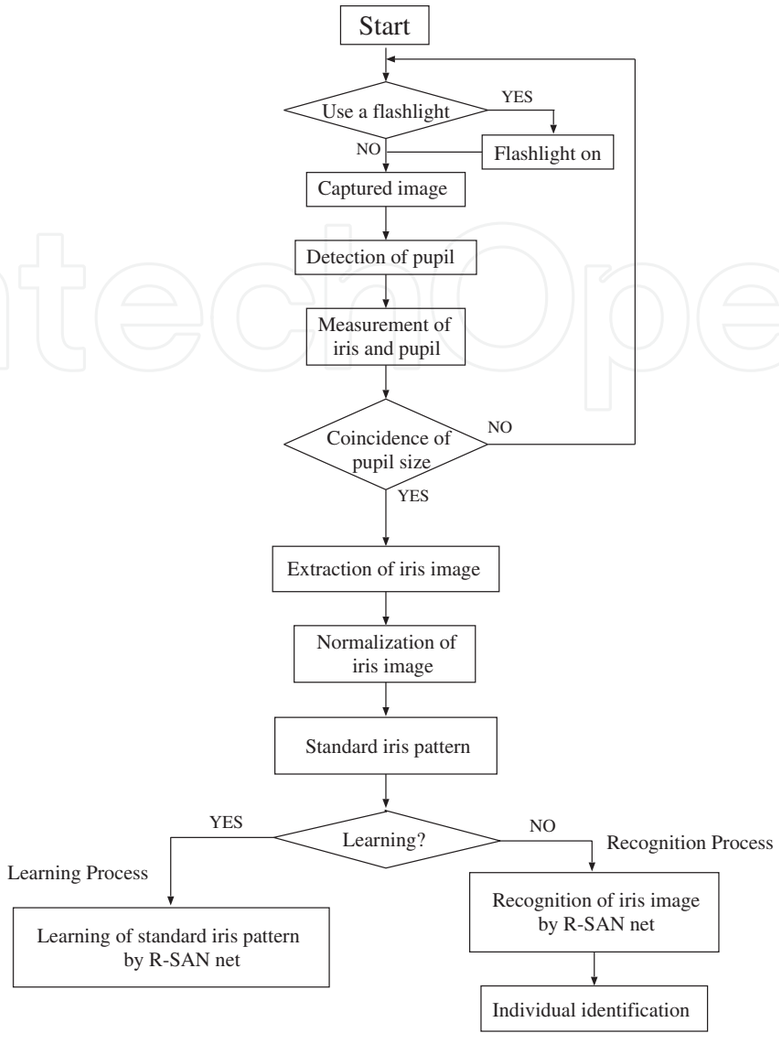

Fig. 7. Flowchart of the iris recognition system.

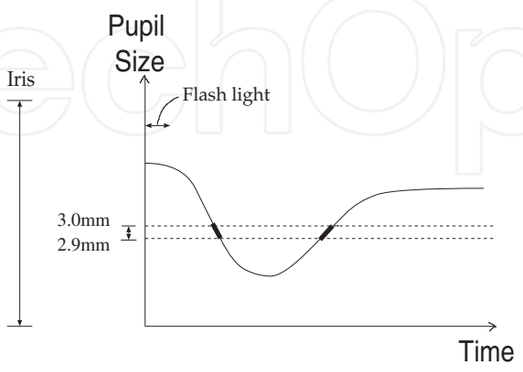

Fig. 8. Variation of pupil diameter caused by pupillary reflex.

between 2.9 mm and 3 mm on the normalized image becomes 50 pixels on the PC screen. The iris size on the screen is also zoomed in the same manner as pupil size normalization. The inset image at the upper left of Fig.9 is a normalized iris image. This normalized image is used as the standard iris pattern which is the input image of the R-SAN net. In the R-SAN net, the standard iris pattern is converted to the transformed pattern on the polar coordinates. In the spreading layer of the R-SAN net, the spread pattern $\boldsymbol{V}$ is obtained by multiplying the transformed pattern by the spreading weight. In learning process, the spread pattern $\boldsymbol{V}_{\mathrm{L}}$ and orientation memory matrix $\mathcal{M}_{\mathrm{O}}$ are stored in the iris recognition system. In recognition process, the orientation angle is obtained by the population vector method using the outputs of orientation recognition neurons. The iris pattern is recognized with the Euclidean distance between the spread patterns obtained in learning and recognition processes.

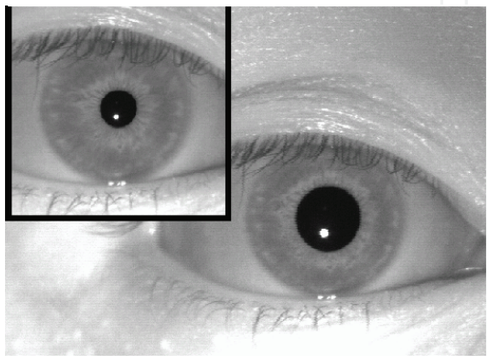

Fig. 9. Size normalization of an iris image.

4. Iris recognition experiment

The characteristics of orientation and shape recognition for learned and unlearned irises were investigated with iris images captured under usual indoor lighting conditions (illuminance was 300 lx). The 38 iris images of 19 subjects (2 images for each subject) were used for recognition experiments. The iris images in the learning and recognition tests were at orientation 0°. One iris image obtained from 19 subjects was used for training. The orientation recognition test was examined using 19 iris images (another iris image of the learned iris and other 18 unlearned irises). We tried 19 sets of recognition tests by changing the learning and recognition iris images one by one. Recognition results were thus obtained for 361 trials consisting of 19 trials for learned subjects and 342 for unlearned subjects. In shape (iris pattern) recognition test, 18 unlearned iris images among 19 subjects were recognized for each learned subject. Thus, 361 recognition trials consisting of 19 trials for learned irises and 342 trials for unlearned irises were examined. The iris pattern recognition was evaluated using the false rejection rate (FRR) and false acceptance rate (FAR). When the output of Euclidean distance for learned iris is higher than the decision threshold, we considered that the person was rejected and calculated the false rejection rate by counting the trials of false rejection. On the other hand, when the output of Euclidean distance calculated for unlearned iris was lower than the decision threshold, we considered that the imposters were accepted incorrectly. We calculated the false acceptance rate by counting the trials of false acceptance.

4.1 Orientation recognition performance

The orientation recognition result for learned and unlearned iris images was shown in Fig.10. The horizontal axis is the input iris number, and the vertical axis is the recognized orientation angle. The average $\pm$ standard deviation of recognized orientation for learned and unlearned irises were $0.82 \pm 2.77[^\circ]$ and $2.01 \pm 62.87[^\circ]$, respectively. As shown in Fig.10, the recognized orientation of learned irises distributed around 0 degree. However, the recognized orientation of unlearned irises was heavily dispersed (SD was very large). The histogram of recognized orientation angle for learned and unlearned irises was shown in Fig.11. The horizontal axis is the absolute error of recognized orientation angle, and the vertical axis is the percentage of iris image included in each bin. The black and white bars show the distribution of the absolute error of recognized orientation for learned and unlearned irises, respectively. The absolute error of recognized orientation for learned irises was less than 5 degrees. However, 87% absolute error of recognized orientation for unlearned irises distributed more than 10 degrees.

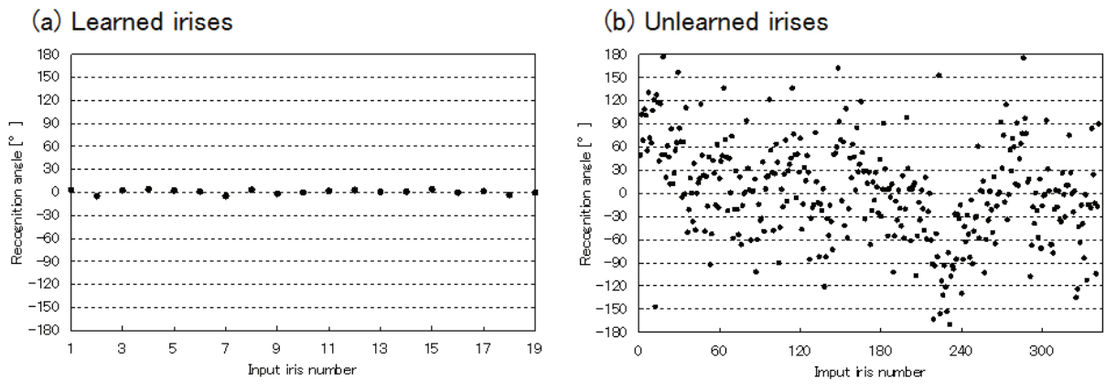

Fig. 10. Orientation recognition result for (a) learned and (b) unlearned irises.

4.2 Shape recognition performance

Shape recognition performance was evaluated using equal error rate (EER) determined by finding the point where false acceptance rate intersects the false rejection rate. The result of shape recognition is shown in Fig.12. The horizontal axis is the decision threshold for discriminating between registered persons and imposters. The vertical axis is the FRR and FAR. Circle and dashed line show the FRR. Square and solid line show the FAR. The equal error rate was 2.02% when the decision threshold of Euclidean distance was 0.33. At the FARs of 1% and 0.1%, the FRRs were 4.01% and 9.58%, respectively.

5. Unlearned iris rejection with recognized orientation

The orientation recognition performances indicated the R-SAN net had fairly good orientation recognition characteristics for learned irises. On the other hand, the orientation angle of unlearned irises was hardly recognized because the distribution of recognized orientation angle was widely dispersive. Thus, the R-SAN net can recognize the orientation of only learned irises. Using the difference of orientation recognition characteristics between learned and unlearned irises, the unlearned iris would be removed before iris discrimination with Euclidean distance. Before iris recognition using Euclidean distance calculated with spread

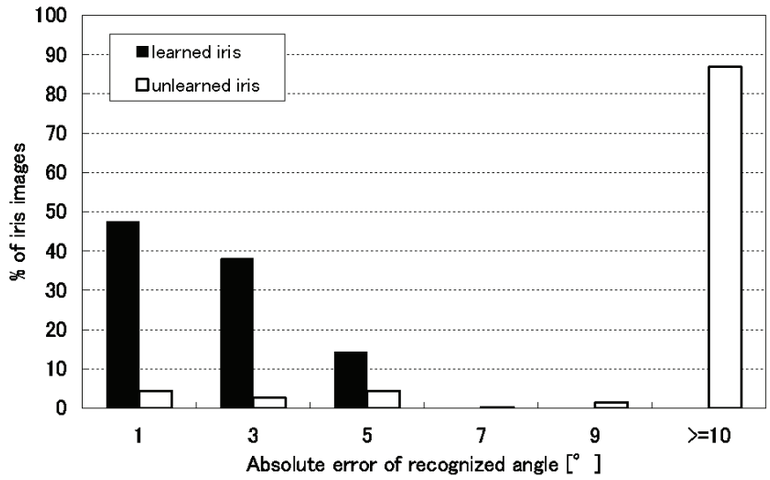

Fig. 11. Histogram of absolute error of recognized orientations for learned and unlearned iris images.

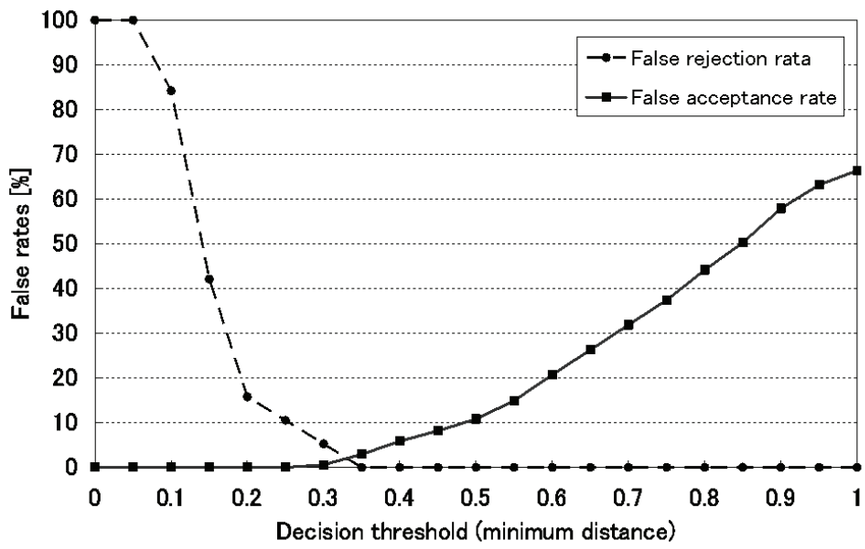

Fig. 12. False acceptance and rejection rates by Euclidean distance.

patterns, the unregistered irises are rejected using the average and standard deviation of recognized orientation angle (θ_{av}, σ_o) for learned irises obtained by the R-SAN net. The input iris was determined as imposter if the recognized orientation is greater than $\theta_{av} + 2.1\sigma_o$ or less than $\theta_{av} - 2.1\sigma_o$. Note that all of learned irises are not rejected with the orientation discrimination because the recognized orientation for learned irises were within $\theta_{av} \pm 2.1\sigma_o$. The shape (iris pattern) recognition performance obtained by new recognition method was shown in Fig.13. The iris images used for learning and recognition are the same as Section 4. This result indicated the FAR drastically decreased. The equal error rate was 0.79% at the decision threshold of 0.34. At the FAR of 1% and 0.1%, the FRR was 0% and 6.95%,

respectively. The unregistered iris rejection by the recognized orientation is very effective to improve the shape recognition performance.

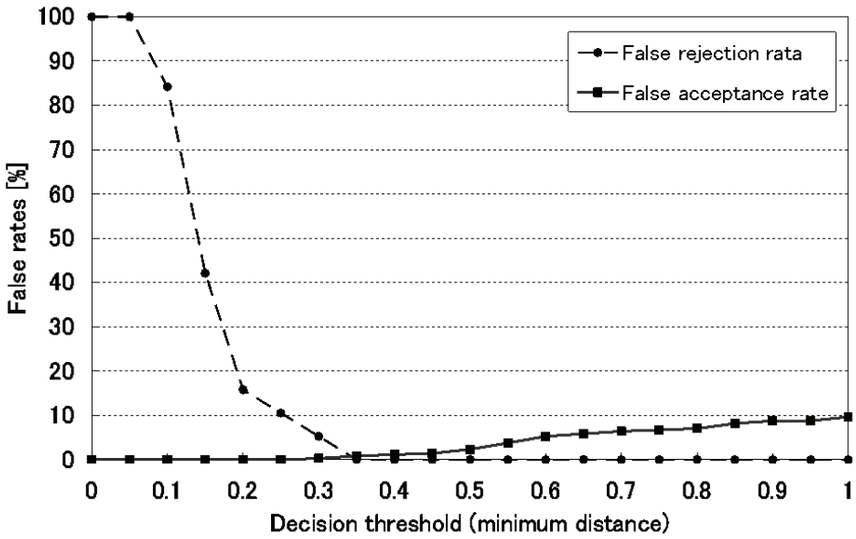

Fig. 13. False acceptance and rejection rates obtained by new iris discrimination method with the characteristics of orientation recognition.

6. Liveness detection using iris pattern

For discriminating between live and fake irises, a new liveness detection method that acquires both liveness and biometric data from the iris portion is introduced. In this method, a variation in the averaged pixel value (brightness) of the iris portion is used as the liveness data. The average brightness is calculated using the pixel values in a predetermined region of the iris portion. The variation in the brightness of the iris portion is caused by a pupillary reflex induced by a weak LED-flashlight. By measuring the variation in the average brightness of the iris portion, the fake iris would be rejected because the fake iris has a constant pattern. However, the brightness varies due to changes in the ambient lighting condition even if the iris pattern does not show a change. Thus, the brightness of the eye image captured by a camera is normalized to prevent a variation in the brightness of the iris image caused by ambient lighting variation (Takano et al., 2007).

In order to discriminate between live and fake irises, it was necessary to investigate the variation rates for live and fake irises. The experiment was performed with 16 images of fake irises, i.e. paper-printed iris images. The brightness variation rates of the live and fake irises are shown in Fig. 14. Trial numbers 1 to 80 shown as triangles represent the brightness variation for fake irises, while trial numbers 81 to 160 shown as circles represent the brightness variation for live irises. The variation rates of the averaged brightness obtained from live and fake irises were 10.6% and 1.5%, respectively. In addition, the maximum brightness variation rate for fake iris images was less than 2.5%. The large difference between the brightness variation rates of live and fake irises provides an anti-deception countermeasure. The decision threshold L_{th} for classification of live and fake irises is obtained by using the brightness variation rates of live and fake irises in Eq.(20). AV_l and AV_f are the average brightness

variation rate of the live and fake irises, respectively. SD_l and SD_f are the standard deviation of brightness variation rate for the live and fake irises, respectively. The decision threshold of the brightness variation rate determined from the present experiment was 3.7%.

$$L_{th} = \frac{AV_l - AV_f}{SD_l + SD_f} SD_f + AV_f \tag{20}$$

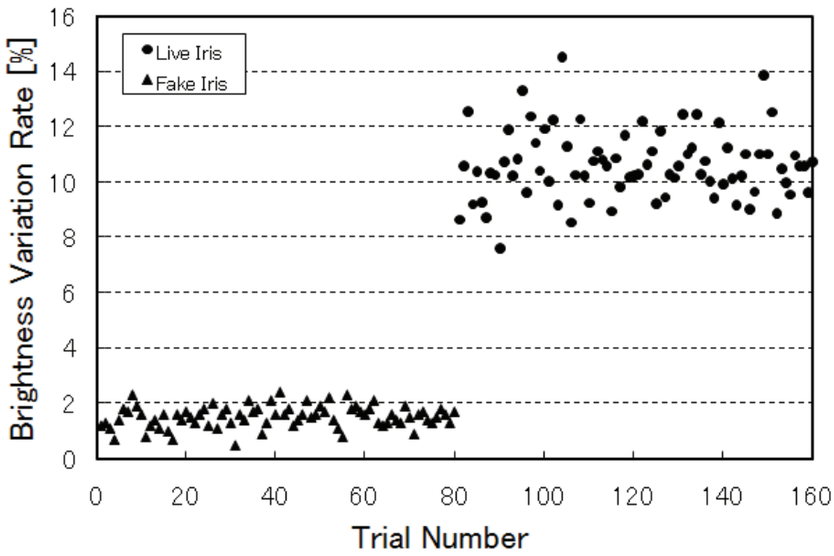

Fig. 14. The characteristics of brightness variation rates obtained from live and fake irises.

7. Conclusions

In this chapter, we showed the orientation and shape recognition performance of the R-SAN net for learned and unlearned irises. The orientation of learned irises can be correctly recognized. On the other hand, the orientation of unlearned irises cannot be recognized because the recognized orientation is heavily dispersed from the orientation of input iris. In the shape recognition with unlearned iris rejection, the equal error rate was 0.79% at decision threshold of 0.34.

The R-SAN net has the unique characteristics of the orientation recognition. The orientation of only learned iris were recognized correctly. However, the recognized orientation of unlearned irises were heavily scattered. By introducing the unlearned iris discrimination with the recognized orientation, new recognition method was developed. The experimental result of new recognition method showed that the false acceptance rate drastically decreased. The unregistered iris rejection method using recognized orientation provided the effective improvement of the iris recognition performance.

The highly reliable liveness detection method by using the average brightness variation of an iris portion based on the pupillary reflex was evaluated with live and fake irises. The averaged brightness variation rate of fake irises was extremely small compared with that of live irises. From the experimental results, the live and fake irises were discriminated with the decision criterion of 3.7% brightness variation rate.

In future work, we will test individual recognition with many more samples of iris patterns. We will also implement the R-SAN net as the security system of the mobile phone, and optimize the orientation and iris pattern recognition algorithms to reduce the computational cost.

8. References

Daugman, J. (1993). High confidence visual recognition of persons by a test of statistical independence. *IEEE Trans. Pattern Anal. Mach. Intell.*, Vol. 15, No. 11, pp. 1148-1161.

Boles, W. & Boashash, B. (1998). A human identification technique using images of the iris and wavelet transform. *IEEE Trans. Signal Process.*, Vol. 46, No. 4, pp. 1185-1188.

Sanchez-Avila, C. & Sanchez-Reillo, R. (2005). Two different approaches for iris recognition using Gabor filters and multiscale zero-crossig representation. *Pattern Recognition*, Vol. 38, No. 2, pp. 231-240.

Wildes, R. P. (1997). Iris recognition: an emerging biometric technology. *Proc. IEEE*, Vol. 85, No. 9, pp. 1348-1363.

Ma, L.; Tan, T.; Wang, Y. & Zhang, D. (2003). Personal identification based on iris texture analysis. *IEEE Trans. Pattern Anal. Mach. Intell.*, Vol. 25, No. 12, pp. 1519-1533.

Ma, L.; Tan, T.; Wang, Y. & Zhang, D. (2004). Local intensity variation analysis for iris recognition. *Pattern Recognition*, Vol. 37, No. 6, pp. 1287-1298.

Ma, L.; Tan, T.; Wang, Y. & Zhang, D. (2004). Efficient iris recognition by characterizing key local variations. *IEEE Trans. Image Process.*, Vol. 13, No. 6, pp. 739-750.

Center for Biometrics and Security Research (2005). CASIA-IrisV4, 09.04.2011, Available from http://www.cbsr.ia.ac.cn/english/IrisDatabase.asp

Sun, Z.; Tan, T. & Qiu, X. (2006). Graph matching iris image blocks with local binary pattern, In: *Advances in Biometrics*, LNCS 3832, pp. 366-372.

Wang, F.; Yao, X. & Han, J. (2007). Minimax probability machine multialgorithmic fusion for iris recognition. *Information Technology Journal*, Vol. 6, No. 7, pp. 1043-1049.

Nakamura, K.; Miyamoto, S. & Morisada, K. (1998). Characteristics of spatial spreading associative neural network in simultaneous recognition of object orientation and shape. *IEICE Trans. Inf. & Syst.*, Vol. J81-D-II, No. 6, pp. 1194-1204.

Yoshikawa, T. & Nakamura, K. (2000). Evaluation of recognition ability and inside parameters for spreading associative neural network. *IEICE Trans. Inf. & Syst.*, Vol. J83-D-II, No. 5, pp. 1332-1343.

Matsumoto, T.; Hirabayashi, M. & Sato, K. (2004). A vulnerability evaluation of iris matching (Part 3). *Proc. The 2004 Symposium on Cryptography and Information Security (SCIS 2004)*, pp. 701-706.

Tachibana, M. (2006). Injustice detection system for iris recognition. *Jpn. Kokai Tokkyo Koho*, No. JP2006-85226 A.

Tsukahara, S. (2006). Iris recognition device. *Jpn. Kokai Tokkyo Koho*, No. JP2006-136450 A.

Oda, T. (2006). Iris code generation system and iris recognition system. *Jpn. Kokai Tokkyo Koho*, No. JP2000-33080 A.

Kobayashi, H.; Takano, H. & Nakamura, K. (2005). Real-time iris recognition system not influenced by ambient light change using a rotation spreading neural network. *IEICE Technical Report*, No. NC2004-163, pp. 155-160.

Kanematsu, M.; Takano, H. & Nakamura, K. (2007). Highly reliable liveness detection method for iris recognition. *Proc. SICE 2007*, pp. 361-364.

Georgopoulus, A. P.; Kalaska, J. F.; Caminiti, R. & Massey, J. T. (1982). On the relations between the direction of two-dimensional arm movements and cell discharge in primate motor cortex. *J. Neurosci.*, Vol. 2, pp. 1527-1537.

Amari, S. (1978). *A Mathematical Principle of Neural Networks*, Sangyo Publishing, Tokyo.

Miyazaki, S.; Takano, H. & Nakamura, K. (2007). Suitable checkpoints of features surrounding the eye for eye tracking using template matching. *Proc. SICE 2007*, pp. 356-360.

Takano, H.; Kobayashi, H. & Nakamura, K. (2007). Rotation invariant iris recognition method adaptive to ambient lighting variation. *IEICE Trans. Inf. & Syst.*, Vol. E90-D, No. 6, pp. 955-962.

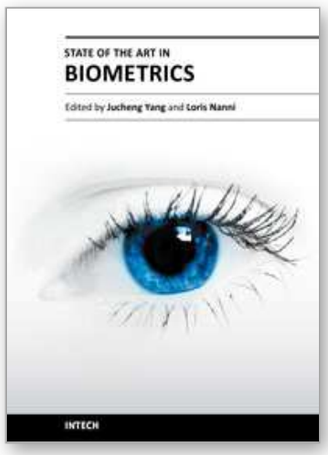

State of the art in Biometrics

Edited by Dr. Jucheng Yang

ISBN 978-953-307-489-4
Hard cover, 314 pages
Publisher InTech
Published online 27, July, 2011
Published in print edition July, 2011

Biometric recognition is one of the most widely studied problems in computer science. The use of biometrics techniques, such as face, fingerprints, iris and ears is a solution for obtaining a secure personal identification. However, the â€œoldâ€ biometrics identification techniques are out of date. This goal of this book is to provide the reader with the most up to date research performed in biometric recognition and descript some novel methods of biometrics, emphasis on the state of the art skills. The book consists of 15 chapters, each focusing on a most up to date issue. The chapters are divided into five sections- fingerprint recognition, face recognition, iris recognition, other biometrics and biometrics security. The book was reviewed by editors Dr. Jucheng Yang and Dr. Loris Nanni. We deeply appreciate the efforts of our guest editors: Dr. Girija Chetty, Dr. Norman Poh, Dr. Jianjiang Feng, Dr. Dongsun Park and Dr. Sook Yoon, as well as a number of anonymous reviewers

InTech Europe
University Campus STeP Ri
Slavka Krautzeka 83/A
51000 Rijeka, Croatia
Phone: +385 (51) 770 447
Fax: +385 (51) 686 166
www.intechopen.com

InTech China
Unit 405, Office Block, Hotel Equatorial Shanghai
No.65, Yan An Road (West), Shanghai, 200040, China
中国上海市延安西路65号上海国际贵都大饭店办公楼405单元
Phone: +86-21-62489820
Fax: +86-21-62489821

IntechOpen